Fractional Disclination Charge and Discrete Shift in the Hofstadter Butterfly

Yuxuan Zhang,[1,2] Naren Manjunath,[1,2] Gautam Nambiar,[1] and Maissam Barkeshli[1,2]
[1]Department of Physics and Joint Quantum Institute, University of Maryland, College Park, Maryland 20742, USA
[2]Condensed Matter Theory Center, University of Maryland, College Park, Maryland 20742, USA

(Received 27 April 2022; accepted 9 November 2022; published 30 December 2022)

In the presence of crystalline symmetries, topological phases of matter acquire a host of invariants leading to nontrivial quantized responses. Here we study a particular invariant, the discrete shift $\mathcal{S}$, for the square lattice Hofstadter model of free fermions. $\mathcal{S}$ is associated with a $\mathbb{Z}_M$ classification in the presence of M-fold rotational symmetry and charge conservation. $\mathcal{S}$ gives quantized contributions to (i) the fractional charge bound to a lattice disclination and (ii) the angular momentum of the ground state with an additional, symmetrically inserted magnetic flux. $\mathcal{S}$ forms its own "Hofstadter butterfly," which we numerically compute, refining the usual phase diagram of the Hofstadter model. We propose an empirical formula for $\mathcal{S}$ in terms of density and flux per plaquette for the Hofstadter bands, and we derive a number of general constraints. We show that bands with the same Chern number may have different values of $\mathcal{S}$, although odd and even Chern number bands always have half-integer and integer values of $\mathcal{S}$, respectively.

DOI: 10.1103/PhysRevLett.129.275301

Topological phases of matter are characterized by invariants that give rise to quantized physical responses, such as the Chern number and associated quantized Hall conductivity. In the presence of spatial symmetries, additional invariants also arise, such as the Wen-Zee shift [1] in clean isotropic continuum quantum Hall systems, which characterizes the response to geometric curvature [2–11]. In order to fully understand systems where lattice effects play an important role, we must develop a complete understanding of invariants and their associated quantized responses for topological phases with charge conservation and crystalline symmetries. Recently, some of the authors [12,13] developed such a systematic theory in two dimensions by analyzing topological terms for crystalline gauge fields and found several additional quantized invariants. Some of these invariants have no continuum analog, while others give a crystalline analog of invariants known from the setting of continuum spatial symmetries.

In this Letter, we study one such invariant, the discrete shift $\mathcal{S}$ and its physical consequences through numerical studies of the square lattice Hofstadter model [14] of spinless free fermions. $\mathcal{S}$ is an invariant that depends on a discrete $\mathbb{Z}_M$ rotational symmetry and U(1) charge conservation and is a discrete analog of the Wen-Zee shift arising in continuum systems. For invertible fermionic topological states [15–17], $2\mathcal{S}$ is an integer defined mod $2M$; we show that, for a fixed Chern number, $\mathcal{S}$ can, in principle, take one of M distinct values, and odd (even) Chern numbers must have half-integer (integer) values of $\mathcal{S}$ [18].

Remarkably, $\mathcal{S}$ refines the known phase diagram of the Hofstadter model, leading to a new Hofstadter butterfly (Fig. 1), which we numerically compute. As we study numerically in detail, $\mathcal{S}$ has a physical manifestation in terms of a quantized contribution to the fractional charge bound to lattice disclinations [see Eq. (2)] and, dually, the fractional angular momentum bound to magnetic flux [see Eq. (4)]. We theoretically justify several properties of $\mathcal{S}$ that are evident from Fig. 1, and also propose an empirical formula for $\mathcal{S}$ [Eq. (5)].

Since the Hofstadter model has now been effectively realized in moiré superlattice systems [19–22], ultracold

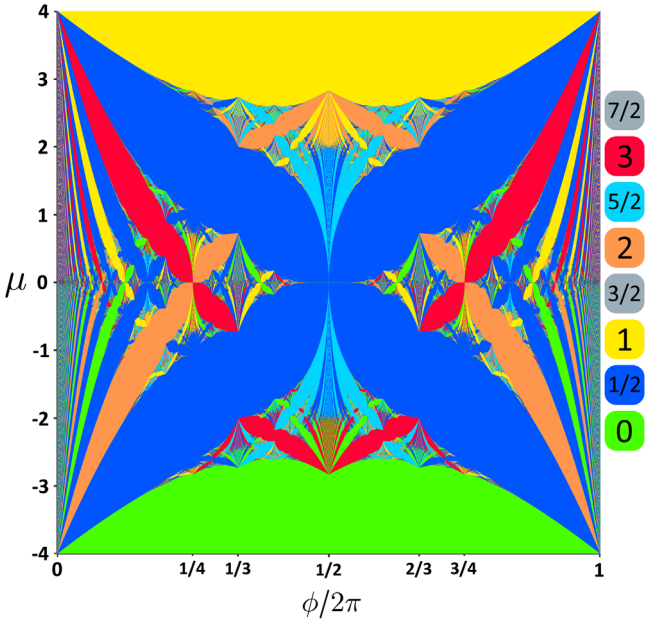

FIG. 1. $\mathcal{S}$ for Hofstadter model, from Eq. (5).

atoms [23–25], and photonics [26,27], an experimental verification of our results may be possible.

We note that [28–34] also study some aspects of the shift in lattice settings, with limited results when Chern number $C \neq 0$, as discussed below and in the Supplemental Material [35], Sec. I.

Model and response theory.—We consider a system of fermions hopping on a lattice with a discrete $\mathbb{Z}_4$ rotational symmetry, a background magnetic flux ϕ per unit cell, and filling ν_0 charge per unit cell. We focus on the Hofstadter model on a square lattice, with the Hamiltonian $H = -t\sum_{\langle i,j\rangle} c_i^\dagger c_j e^{-iA_{bgd;ij}} + \text{H.c.}$ This describes spinless free fermions c_i coupled to a background U(1) gauge field A_{bgd}, whose holonomy around each plaquette is ϕ. When $\phi = 2\pi(p/q)$ with coprime integers p and q, the system has q bands. When r bands are filled, $\nu_0 = r/q$. At any gapped point in the parameter space (ν_0, ϕ), the total Chern number C of the filled bands is determined by the conditions $\nu_0 = (p/q)C \bmod 1$; $|C| \leq (q/2)$ [44]. Each connected gapped region in this parameter space has a fixed value of C. Simply connected gapped regions with Chern number C (referred to as Chern number C lobes) are separated by special values of $(\phi/2\pi)$ which lie in the Farey sequence of order $2|C|$ [45]. The continuum limit of n filled Landau levels is obtained by taking $(p/q) \to 0^+$ and $C = n$.

H has a symmetry group G, which is a central extension of the wallpaper group $p4 = \mathbb{Z}^2 \rtimes \mathbb{Z}_4$ by U(1). This means that the magnetic translations are generated by the many-body operators $T_{\mathbf{x}}$, $T_{\mathbf{y}}$, which satisfy $T_{\mathbf{x}}T_{\mathbf{y}} = T_{\mathbf{y}}T_{\mathbf{x}}e^{i\phi\hat{N}}$, where $\hat{N}$ is the total particle number operator. The Hamiltonian is invariant under a "magnetic" rotation operator $\tilde{C}_{4,\lambda} \equiv \hat{C}_4 e^{i\sum_j \lambda_j c_j^\dagger c_j}$, where λ_j is a gauge transformation at site j, which is fixed up to an overall constant by A_{bgd}. The usual rotation operator $\hat{C}_4$ acts as $\hat{C}_4 c_j \hat{C}_4^\dagger = c_{R(j)}$, where $R(j)$ is a vertex-centered $\pi/2$ rotation of site j.

The quantized universal properties can be encoded by a topological response theory involving a background G gauge field $B = (\delta A, \vec{R}, \omega)$, which is nonabelian [12]. Here $\delta A = A - A_{bgd}$ is the deviation of the total U(1) gauge field A relative to A_{bgd}, while $\omega, \vec{R}$ are the crystalline gauge fields (see Supplemental Material [35], Sec. VII for additional details, which includes Refs. [36–42]). ω is a background gauge field for the $\mathbb{Z}_4$ rotational symmetry; in the continuum limit, it is identified with the spin connection. $\vec{R}$ is a two-component gauge field for the $\mathbb{Z}^2$ translational symmetry. In terms of $\vec{R}$ and ω we also define an area element A_{XY}, which counts the number of unit cells [12]. Note that the integral $\delta\Phi_W \equiv \int_W d\delta A$ over a two-dimensional region W gives the total excess magnetic flux within W, not including the background flux, while $\int_W d\omega$ gives the total disclination angle of disclinations within W. ω and $\vec{R}$ are taken to be real-valued fields with quantized periods, since they are $\mathbb{Z}_4$ and $\mathbb{Z}^2$ gauge fields, respectively [46].

We can write all terms in the topological response theory that depend on A or ω [12],

$$\mathcal{L} = \frac{C}{4\pi} A \wedge dA + \frac{\mathcal{S}}{2\pi} A \wedge d\omega + \frac{\vec{\mathscr{P}}_c}{2\pi} \cdot A \wedge \vec{T} + \frac{k_0}{2\pi} A \wedge A_{XY} + \frac{\tilde{\ell}_s}{4\pi} \omega \wedge d\omega + \frac{\vec{\mathscr{P}}_s}{2\pi} \cdot \omega \wedge \vec{T} + \frac{k_s}{2\pi} \omega \wedge A_{XY}. \tag{1}$$

See Supplemental Material [35], Sec. VII for a discussion. $\vec{T} = d\vec{R} + i\sigma_y \omega \wedge \vec{R}$ is the torsion two-form. Here C and $2\mathcal{S}$ must be quantized to integers. For fermionic invertible phases there are some additional terms in the theory, discussed in the Supplemental Material [35], Sec. VII. The first term defines the Hall conductivity $\bar{\sigma}_H = (C/2\pi)$ in natural units and assigns charge to flux. The second term assigns a fractional U(1) charge $\mathcal{S}(\Omega/2\pi)$ to a defect with disclination angle Ω. On a square lattice, it is topologically trivial if a $(\pi/2)$ disclination is assigned an integer charge, which can be removed by applying local operators at the disclination core. Thus, only $\mathcal{S}$ mod 4 is a symmetry-protected invariant, in contrast to the continuum shift, which is a $\mathbb{Z}$ invariant [47]. The second term can also be written as $(\mathcal{S}/2\pi)\omega \wedge dA$, which assigns angular momentum $\mathcal{S}(dA/2\pi)$ to flux dA. In the Supplemental Material [35], Sec. VIII we show the nontrivial result that for spinless fermions in free or interacting systems, $\mathcal{S}$ is quantized to a half-integer if C is odd and to integers if C is even. The numerical values of $\mathcal{S}$ in Fig. 1 agree with this result.

$\nu_0 = C(\phi/2\pi) + k_0$ and $\nu_s = \mathcal{S}(\phi/2\pi) + k_s$ are the charge and angular momentum per unit cell, with k_0 and k_s as integers. The terms with $\vec{T}$ in Eq. (1) can be detected by inserting defects with nontrivial dislocation Burgers vector, but we do not consider such defects in this Letter. Hereafter, we ignore these, as well as the $\omega \wedge d\omega$ term.

Fractional disclination charge.—Equation (1) predicts a contribution to the charge localized at a $(\pi/2)$ disclination coming from $\mathcal{S}$. Here we compare the field theory prediction to microscopic calculations. The discussion below applies to general lattices with $p4$ space group symmetry.

We construct a $(\pi/2)$ disclination at the point o by deleting a quadrant from the infinite plane and reconnecting sites using the operator $\tilde{C}_{4,\lambda}$ (see Supplemental Material [35], Sec. III, which includes Ref. [43]). In particular, if each unit cell in the disclination lattice has the same flux, we show that $\lambda_o = 0$. Now consider a region W enclosing the disclination, such that the distance between the disclination and the boundary ∂W is much greater than the correlation length. The total charge is

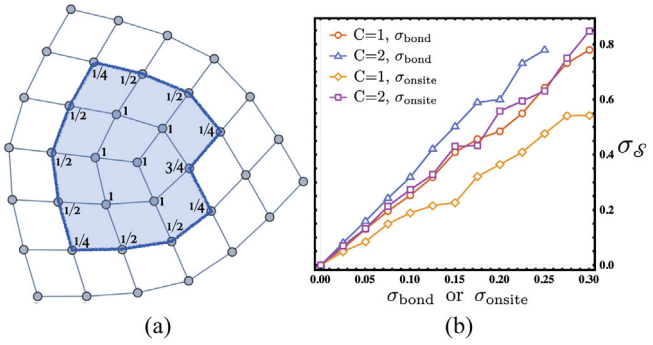

FIG. 2. (a) Lattice disclination with disclination angle $\Omega = (\pi/2)$. The blue region W covers 11 unit cells. Q_i is weighted by the indicated amount when calculating Q_W or $\bar{Q}_W$. (b) Standard deviation of $\mathcal{S}$ as a function of bond disorder σ_{bond} or on site disorder $\sigma_{\text{on site}}$ for $C = 1$ and $C = 2$ main Landau level (average hopping is one).

$$Q_W = \int_W \frac{\delta\mathcal{L}}{\delta A_0} = C\frac{\delta\Phi_W}{2\pi} + \mathcal{S}\frac{\Omega_W}{2\pi} + \nu_0 n_{u.c.,W}, \quad (2)$$

where $n_{u.c.,W}$, Ω_W, and $\delta\Phi_W$ are the number of unit cells in W, disclination angle, and excess magnetic flux (on top of the background flux $n_{u.c.,W}\phi$), respectively. Here we use that $\int_W dA = \delta\Phi_W + n_{u.c.,W}\phi$ and $v_0 = C\phi/2\pi + k_0$. In order to use Eq. (2), W should enclose a definite integer number of unit cells. Furthermore, in order to ensure that the condition $Q_W + Q_{W'} = Q_{W\cup W'}$ holds microscopically, as in the field theory, we define $Q_W \equiv \sum_{i\in W} \text{wt}(i) Q_i$ where the weight $\text{wt}(i) = 1$ for interior points and $\text{wt}(i) = \frac{1}{4}, \frac{2}{4}, \frac{3}{4}$ if the interior of W subtends an angle $(\pi/2), \pi, (3\pi/2)$ at site i [see Fig. 2(a)]. Note that our definition of disclination charge differs from previous work [30].

The charge on a site Q_i is simply $\langle c_i^\dagger c_i\rangle$ in the ground state. We choose W such that it encloses a single disclination with $\Omega_W = (\pi/2)$. We set the excess flux $\delta\Phi_W = 0$ in our numerics. ν_0 can be defined as the filling of a corresponding clean lattice on a torus with the same flux per unit cell ϕ. On a lattice with disclinations, ν_0 is also the charge per unit cell far away from the disclination. Suppose we define the excess charge in W as $\bar{Q}_W \equiv Q_W - \nu_0 n_{u.c.,W}$. We can then extract the shift $\mathcal{S}$ to be $(\mathcal{S}/4) = \bar{Q}_W$. Numerically, we find that $\bar{Q}_W$, and hence the computed $\mathcal{S}$, is indeed independent of the size of W for large enough W. We show this by explicitly plotting Q_i and the size dependence of $\bar{Q}_W$ for three representative sets of parameters in the Hofstadter butterfly (Fig. 3). We can thus use this procedure to calculate $\mathcal{S}$ throughout the Hofstadter butterfly; this is shown in Fig. 1. In the Landau level limit, we numerically recover the result $\mathcal{S} = (C^2/2)$ [1].

It is instructive to apply Eq. (2) when W is the entire surface of a cube, which has eight $(\pi/2)$ disclinations corresponding to the eight corners. In this case, we obtain

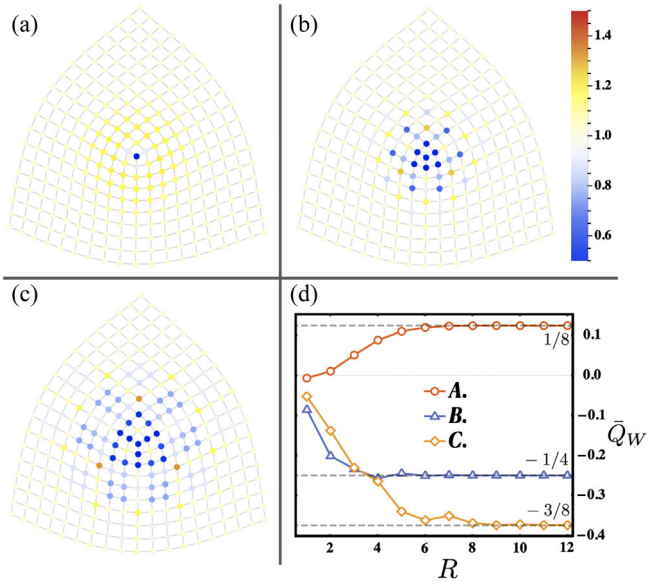

FIG. 3. (a)–(c) Q_i for each site i in a clean system with parameters (a) $(\phi/2\pi) = \epsilon$, $C = 1$, (b) $(\phi/2\pi) = \frac{1}{2} - \epsilon$, $C = -2$, (c) $(\phi/2\pi) = \frac{1}{3} + \epsilon$, $C = 3$. The color bar is in units of ν_0. ϵ is a small fraction that opens up the band gap. (d) $\bar{Q}_W$ for (a)–(c) is quantized at $(\mathcal{S}/4)$ when $R \geq 9$. R is the distance from the disclination center to ∂W (total side length is $L = 24$ unit cells). Here we have cropped out the edges to show the bulk features more clearly; the full figures with edges are given in the Supplemental Material [35], Sec. V.

$$Q_{\text{cube}} = 2\mathcal{S} + \nu_0 n_{u.c.,\text{cube}}. \quad (3)$$

Thus, in order to be in the same gapped phase as a state on a torus with filling ν_0 and identical ϕ and Chern number C, the total charge on the cube is shifted from the naïve expectation of $\nu_0 n_{u.c.,\text{cube}}$ by $2\mathcal{S}$. Numerically, this agrees with the number of extra single particle states we need to fill.

Note that the weighting procedure and the numerical result $\bar{Q}_W = (\mathcal{S}/4)$ generalize to any C_4 symmetric lattice. The details are described in the Supplemental Material [35], Sec. V.

Let us now introduce bond and on site potential disorder, which break the crystalline symmetry. In this case, the value of $\mathcal{S}$ extracted from $\bar{Q}_W$ through $\mathcal{S} = 4\bar{Q}_W$ deviates from its quantized value for each disorder realization, although it remains quantized after disorder averaging. The standard deviation $\sigma_{\mathcal{S}}$ computed from $\bar{Q}_W$ grows to order 1 with an increase in disorder strength, as shown for two representative lobes in Fig. 2(b). The value of $\mathcal{S}$ extracted from Q_{cube} is much more robust (i.e., much smaller standard deviation) as long as the chemical potential is far from the band edge, since in this case Q_{cube} can change only if a given disorder configuration moves a single particle state across the chemical potential.

Angular momentum due to flux.—Since ω is a rotation gauge field, the angular momentum is the charge

under rotations, given by $l = \int(\delta\mathcal{L}/\delta\omega_0) = \mathcal{S}[(\delta\Phi/2\pi) + (\phi/2\pi)n_{u.c.}] + k_s n_{u.c.}$ mod 4. Below, we compare this topological field theory (TFT) prediction to microscopic calculations. Consider the Hofstadter Hamiltonian on an $L \times L$ torus, with L even and ϕ flux per plaquette. By turning on δA, we add a flux $2\pi\Delta m$, also distributed uniformly. If the system has Chern number C, we fill ΔmC additional single particle states in order to get a gapped many-body state with the same C. This state has $m = (\phi L^2/2\pi) + \Delta m$ flux quanta.

We use the same magnetic rotation operator $\tilde{C}_{4,\lambda}$ that we used to define the disclination. This means that we require $\lambda_o = 0$, where o is a fixed point of the rotation.

Note that the holonomies $e^{-i\oint(\delta A + A_{bgd})\cdot dl}$ along the two noncontractible cycles of the torus are position dependent. Translation by one site changes the holonomy by a factor $e^{i2\pi(m/L)}$ and is therefore an exact symmetry only for the infinite system; for any finite system, translation by one site can only be an approximate symmetry. On a finite size torus with even L, there are two points, o_1 and o_2, distinguished by having holonomy 1 or $e^{i\pi m}$ along both directions. The vertex-centered $\pi/2$ rotational symmetry is only exact for a finite size system when o_1 and o_2 are both fixed points of this rotation.

Since we have two distinct fixed points o_1 and o_2, there are two distinct choices of gauge satisfying the above condition, either $\lambda_{o_1} = 0$ and $\lambda_{o_2} = m(\pi/2)$, or $\lambda_{o_2} = 0$ and $\lambda_{o_1} = -m(\pi/2)$. In what follows, we pick the first choice, denoted $\tilde{C}_4$; the second is related by an overall U(1) rotation $e^{-i\hat{N}m(\pi/2)}$, as will be discussed in the Supplemental Material [35], Sec. VI.

The many-body ground state $|\Psi_m\rangle$ satisfies $\tilde{C}_4|\Psi_m\rangle = e^{il(m)(\pi/2)}|\Psi_m\rangle$. Since $\tilde{C}_4^4 = 1$, $l(m)$ is an integer mod 4.

In this setup, we require each rotation center to be a vertex. On a torus, this forces L to be even: if L were odd, any rotation would leave two points invariant, one at a vertex and the other at a plaquette center. If the rotation center was at a plaquette center, then the original $\tilde{C}_4$ rotation would be modified by a lattice translation. The associated eigenvalue would receive a contribution from the $A \wedge \vec{T}$ term in Eq. (1), which we do not wish to consider here. Indeed, the numerical result with plaquette centered rotations is not consistent with Fig. 1.

We find from direct numerical calculation,

$$l(m) = \mathcal{S}m + C\frac{m^2}{2} + K(C, L) \quad \text{mod } 4. \tag{4}$$

The quadratic dependence on m is beyond the TFT description; while it is well-known from the continuum Landau level problem, it has not been derived using effective field theory [48]. For a given lobe, $K(C, L)$ is an integer that does not depend on m, but does depend on C and L. We can obtain $\mathcal{S}$ by subtracting the quadratic term and taking the difference: $\mathcal{S} = l(m+1) - l(m) - Cm - (C/2)$ mod 4. For each lobe with a given C, the value of $\mathcal{S}$ obtained from Eq. (4) matches the result using Eq. (3), confirming the expected duality.

Instead of inserting additional Δm flux uniformly everywhere, we can insert it locally in a smaller region W symmetrically around the rotation center. We find that the value of $\mathcal{S}$ remains constant for different sizes of W, even in the limit when W contains just four plaquettes (when C is small enough).

We can also extract $\mathcal{S}$ using *partial* rotations [31,49]. That is, in a system with background flux $2\pi m_0$ we insert a local flux of $2\pi\Delta m$ in a region W, and we compute $\langle\Psi_{\Delta m,m_0}|\tilde{C}_4|_D|\Psi_{\Delta m,m_0}\rangle$, where $\tilde{C}_4|_D$ is the restriction of $\tilde{C}_4$ to a region D containing W and $|\Psi_{\Delta m,m_0}\rangle$ is the ground state. Let us fix W and D to be centered on o_2 and continue with our previous gauge choice $\lambda_{o_1} = 0$. The ground state expectation value can be written as $\langle\Psi_{\Delta m,m_0}|\tilde{C}_4|_D|\Psi_{\Delta m,m_0}\rangle = e^{-\gamma_D(\Delta m,m_0)+il_D(\Delta m,m_0)\pi/2}$. The magnitude $e^{-\gamma_D(\Delta m,m_0)}$ has an exponentially decaying envelope as the perimeter ∂D increases, as expected, in addition to an oscillatory behavior that we do not study in detail. We empirically find $l_D(\Delta m, m_0) = l_D(0, m_0) + \mathcal{S}\Delta m + Cm\Delta m + [C(\Delta m)^2/2]$ mod 4. This matches the expectation from Eq. (4). One can also perform the partial rotation computation in the case where the total system is defined with open boundary conditions, as discussed in the Supplemental Material [35], Sec. VI.

On the torus, we find that the formula for $l_D(\Delta m, m_0) - l_D(0, m_0)$ is sensitive in complicated ways to the gauge choice $\lambda_{o_1} = 0$ or $\lambda_{o_2} = 0$ and whether D is centered on o_1 or o_2; these dependencies are not fully understood. We discuss this and related issues arising for open boundary conditions in the Supplemental Material [35], Sec. VI.

Theoretical analysis.—As a function of μ and ϕ, $\mathcal{S}$ and C have the following general properties (note $\mathcal{S}$ is defined mod 4): (1) $\mathcal{S}$ mod $1 = (C/2)$ mod 1. (2) $\mathcal{S}(\mu, \phi) = \mathcal{S}(\mu, 2\pi - \phi)$, i.e., $\mathcal{S}$ is invariant under time reversal. (3) For the bands with the same Chern number C, $\mathcal{S}(\mu, \phi) = 1 - \mathcal{S}(-\mu, \phi)$. (4) When $\mathcal{S}$ changes, $(\phi/2\pi)$ must lie in the Farey sequence of order $|C|$. (5) $\mathcal{S}(\mu, 0^+) = (C^2/2)$ for $C > 0$.Properties (1–3) will be justified in the Supplemental Material [35], Sec. VIII. We explain (1) also for general interacting systems, using the classification of invertible topological phases in Ref. [15]. Property (2) follows for general interacting systems from the time-reversal invariance of the field theory term $\omega \wedge dA$, while (5) reproduces the known results in the continuum Landau level limit [1].

Now let us explain property (4). Consider all possible fractions (p/q) with $0 \le (p/q) \le 1$ and $1 \le q \le 2|C|$ and p, q coprime. Arrange them in increasing order, with zero being the first element and one being the last. The resulting sequence is called the "Farey sequence" of order $2|C|$. Now, the different lobes with Chern number C are uniquely

specified by the intervals of $(\phi/2\pi)$ obtained from this sequence [45]. Moreover, each lobe has a constant value of shift. In our numerics, when $\mathcal{S}$ jumps, $\phi/2\pi$ must lie at fractions (p/q) in a smaller set, namely, the Farey sequence of order $|C|$; see Supplemental Material [35], Sec. II.

Empirical formula for $\mathcal{S}$.—Suppose we fix a $C > 0$ and consider $\mathcal{S}(\phi)$ as $(\phi/2\pi) = (p/q)$ is increased from 0 to 1. As stated above, $\mathcal{S}(\phi)$ jumps by integers at specific values of (p/q), where $q \leq |C|$. At a given (p/q), the total jump, defined as $\lim_{\epsilon\to 0^+} \mathcal{S}[2\pi(p/q)+\epsilon] - \mathcal{S}[2\pi(p/q)-\epsilon]$, is the sum of two contributions: A contribution of $-C-1$ whenever q divides C and another contribution of $2\lfloor (C+q)/2q \rfloor$ whenever q is odd. Both contributions are automatically zero if $q > |C|$. The observed jumps are tabulated in the Supplemental Material [35], Sec. II, up to $C = 12$. From these observations, we propose the following empirical formula by summing over all jumps that occur at $2\pi(p/q) < \phi$. For $C > 0$,

$$\mathcal{S}(\phi) = \frac{C^2}{2} - (C+1)\left\lfloor \frac{C\phi}{2\pi} \right\rfloor + 2\sum_{\substack{\frac{p}{q} < \frac{\phi}{2\pi} \\ \text{odd } q}} \left\lfloor \frac{C+q}{2q} \right\rfloor \mod 4, \tag{5}$$

where in the third term we sum over all (p/q) in the Farey sequence of order C that satisfy $(p/q) < (\phi/2\pi)$ and q odd. $\mathcal{S}$ for $C < 0$ can be obtained from the symmetry transformation $\mathcal{S}(\mu,\phi) = 1 - \mathcal{S}(-\mu,\phi)$, which flips the sign of C. We numerically checked Eq. (5) for all $|C| \leq 7$ lobes using Eq. (3) on a cube of side length $L = 28$. We also checked all $|C| \leq 12$ lobes using Eq. (4) on a torus with side length $L = 140$, and we checked some representative $|C| = 45$ lobes with $L = 180$. We use (5), together with an eigenvalue database [45], to generate Fig. 1.

Lobes with the same (C, k_0) can have distinct values of $\mathcal{S}$. For example, when $(C, k_0) = (4, -1)$ we can take $(\phi/2\pi) = 1/3 \mp \epsilon$ and find $\mathcal{S} = 3, 1 \bmod 4$, respectively. Also note that, in Fig. 1, we do not see any bands with total shift $\mathcal{S} = 3/2$ or $7/2$. However, there is no theoretical obstruction to realizing this in a system with odd C. Indeed, there are several examples of single excited bands that have odd C and $\mathcal{S} = 3/2$ or $7/2$ in this model.

We thank M. Hafezi and S. Das Sarma for comments on the draft and V. Galitski and D. Bulmash for discussions on related projects. This work is supported by the Laboratory for Physical Sciences through the Condensed Matter Theory Center, NSF CAREER (DMR-1753240) (M. B., N. M.), ARO W911NF-20-1-0232 (G. N.).

[1] X. G. Wen and A. Zee, Shift and Spin Vector: New Topological Quantum Numbers for the Hall Fluids, Phys. Rev. Lett. **69**, 953 (1992).

[2] J. E. Avron, R. Seiler, and P. G. Zograf, Viscosity of Quantum Hall Fluids, Phys. Rev. Lett. **75**, 697 (1995).

[3] N. Read, Non-Abelian adiabatic statistics and Hall viscosity in quantum Hall states and $p_x + ip_y$ paired superfluids, Phys. Rev. B **79**, 045308 (2009).

[4] N. Read and E. H. Rezayi, Hall viscosity, orbital spin, and geometry: Paired superfluids and quantum Hall systems, Phys. Rev. B **84**, 085316 (2011).

[5] F. D. M. Haldane, "Hall viscosity" and intrinsic metric of incompressible fractional hall fluids, arXiv:0906.1854.

[6] F. D. M. Haldane, Geometrical Description of the Fractional Quantum Hall Effect, Phys. Rev. Lett. **107**, 116801 (2011).

[7] A. G. Abanov and A. Gromov, Electromagnetic and gravitational responses of two-dimensional noninteracting electrons in a background magnetic field, Phys. Rev. B **90**, 014435 (2014).

[8] B. Bradlyn and N. Read, Low-energy effective theory in the bulk for transport in a topological phase, Phys. Rev. B **91**, 125303 (2015).

[9] A. Gromov, G. Y. Cho, Y. You, A. G. Abanov, and E. Fradkin, Framing Anomaly in the Effective Theory of the Fractional Quantum Hall Effect, Phys. Rev. Lett. **114**, 016805 (2015).

[10] N. Schine, A. Ryou, A. Gromov, A. Sommer, and J. Simon, Synthetic Landau levels for photons, Nature (London) **534**, 671 (2016).

[11] Y.-H. Wu, H.-H. Tu, and G. J. Sreejith, Fractional quantum Hall states of bosons on cones, Phys. Rev. A **96**, 033622 (2017).

[12] N. Manjunath and M. Barkeshli, Crystalline gauge fields and quantized discrete geometric response for Abelian topological phases with lattice symmetry, Phys. Rev. Res. **3**, 013040 (2021).

[13] N. Manjunath and M. Barkeshli, Classification of fractional quantum Hall states with spatial symmetries, arXiv:2012.11603.

[14] D. R. Hofstadter, Energy levels and wave functions of Bloch electrons in rational and irrational magnetic fields, Phys. Rev. B **14**, 2239 (1976).

[15] M. Barkeshli, Y.-A. Chen, P.-S. Hsin, and N. Manjunath, Classification of $(2+1)$D invertible fermionic topological phases with symmetry, Phys. Rev. B **105**, 235143 (2022).

[16] D. S. Freed and M. J. Hopkins, Reflection positivity and invertible topological phases, Geom. Topol. **25**, 1165 (2021).

[17] D. Aasen, P. Bonderson, and C. Knapp, Characterization and classification of fermionic symmetry enriched topological phases, arXiv:2109.10911.

[18] For invertible bosonic topological states, $\mathcal{S}$ must be an integer, while for fractionalized topological states, $\mathcal{S}$ can be fractional.

[19] C. R. Dean *et al.*, Hofstadter's butterfly and the fractal quantum Hall effect in moiré superlattices, Nature (London) **497**, 598 (2013).

[20] B. Hunt, J. D. Sanchez-Yamagishi, A. F. Young, M. Yankowitz, B. J. LeRoy, K. Watanabe, T. Taniguchi, P. Moon, M. Koshino, P. Jarillo-Herrero, and R. C. Ashoori, Massive Dirac fermions and Hofstadter butterfly in a van der Waals heterostructure, Science **340**, 1427 (2013).

[21] Y. Saito, J. Ge, L. Rademaker, K. Watanabe, T. Taniguchi, D. A. Abanin, and A. F. Young, Hofstadter subband ferromagnetism and symmetry-broken Chern insulators in twisted bilayer graphene, Nat. Phys. **17**, 478 (2021).
[22] E. M. Spanton, A. A. Zibrov, H. Zhou, T. Taniguchi, K. Watanabe, M. P. Zaletel, and A. F. Young, Observation of fractional Chern insulators in a van der Waals heterostructure, Science **360**, 62 (2018).
[23] M. Aidelsburger, M. Atala, M. Lohse, J. T. Barreiro, B. Paredes, and I. Bloch, Realization of the Hofstadter Hamiltonian with Ultracold Atoms in Optical Lattices, Phys. Rev. Lett. **111**, 185301 (2013).
[24] H. Miyake, G. A. Siviloglou, C. J. Kennedy, W. C. Burton, and W. Ketterle, Realizing the Harper Hamiltonian with Laser-Assisted Tunneling in Optical Lattices, Phys. Rev. Lett. **111**, 185302 (2013).
[25] C. J. Kennedy, W. C. Burton, W. C. Chung, and W. Ketterle, Observation of Bose–Einstein condensation in a strong synthetic magnetic field, Nat. Phys. **11**, 859 (2015).
[26] M. Hafezi, S. Mittal, J. Fan, A. Migdall, and J. M. Taylor, Imaging topological edge states in silicon photonics, Nat. Photonics **7**, 1001 (2013).
[27] T. Ozawa, H. M. Price, A. Amo, N. Goldman, M. Hafezi, L. Lu, M. C. Rechtsman, D. Schuster, J. Simon, O. Zilberberg, and I. Carusotto, Topological photonics, Rev. Mod. Phys. **91**, 015006 (2019).
[28] R. R. Biswas and D. T. Son, Fractional charge and inter-Landau–level states at points of singular curvature, Proc. Natl. Acad. Sci. U.S.A. **113**, 8636 (2016).
[29] S. Liu, A. Vishwanath, and E. Khalaf, Shift Insulators: Rotation-Protected Two-Dimensional Topological Crystalline Insulators, Phys. Rev. X **9**, 031003 (2019).
[30] T. Li, P. Zhu, W. A. Benalcazar, and T. L. Hughes, Fractional disclination charge in two-dimensional C_n-symmetric topological crystalline insulators, Phys. Rev. B **101**, 115115 (2020).
[31] Y. You, J. Bibo, and F. Pollmann, Higher-order entanglement and many-body invariants for higher-order topological phases, Phys. Rev. Res. **2**, 033192 (2020).
[32] J. May-Mann and T. L. Hughes, Crystalline responses for rotation-invariant higher-order topological insulators, arXiv:2108.00008.
[33] C. W. Peterson, T. Li, W. Jiang, T. L. Hughes, and G. Bahl, Trapped fractional charges at bulk defects in topological insulators, Nature (London) **589**, 376 (2021).
[34] B. Han, H. Wang, and P. Ye, Generalized Wen-Zee terms, Phys. Rev. B **99**, 205120 (2019).
[35] See Supplemental Material at http://link.aps.org/supplemental/10.1103/PhysRevLett.129.275301 for further details on the field theory and the numerics, which includes Refs. [36–43].
[36] A. Kapustin, Bosonic topological insulators and paramagnets: A view from cobordisms, arXiv:1404.6659.
[37] E. Witten, Quantum field theory and the Jones polynomial, Commun. Math. Phys. **121**, 351 (1989).
[38] R. Thorngren and D. V. Else, Gauging Spatial Symmetries and the Classification of Topological Crystalline Phases, Phys. Rev. X **8**, 011040 (2018).
[39] A. Debray, Invertible phases for mixed spatial symmetries and the fermionic crystalline equivalence principle, arXiv:2102.02941.
[40] Q.-R. Wang and Z.-C. Gu, Construction and Classification of Symmetry-Protected Topological Phases in Interacting Fermion Systems, Phys. Rev. X **10**, 031055 (2020).
[41] D. V. Else and R. Thorngren, Crystalline topological phases as defect networks, Phys. Rev. B **99**, 115116 (2019).
[42] J.-H. Zhang, S. Yang, Y. Qi, and Z.-C. Gu, Real-space construction of crystalline topological superconductors and insulators in 2d interacting fermionic systems, arXiv:2012.15657.
[43] M. Barkeshli, P. Bonderson, M. Cheng, and Z. Wang, Symmetry fractionalization, defects, and gauging of topological phases, Phys. Rev. B **100**, 115147 (2019).
[44] D. J. Thouless, M. Kohmoto, M. P. Nightingale, and M. den Nijs, Quantized Hall Conductance in a Two-Dimensional Periodic Potential, Phys. Rev. Lett. **49**, 405 (1982).
[45] D. Osadchy and J. E. Avron, Hofstadter butterfly as quantum phase diagram, J. Math. Phys. (N.Y.) **42**, 5665 (2001).
[46] One can also work in a simplicial formulation where ω and $\vec{R}$ are taken to have discrete values [12].
[47] Note that the conventional definition of shift in the quantum Hall literature is $S \equiv \chi(\mathcal{S}/\bar{\sigma}_H)$, with χ as the Euler characteristic of the space.
[48] Liu *et al.* [29] accounted for the m^2 contribution in terms of the angular momentum of the electromagnetic field, however, physically this term arises from the electron fluid itself.
[49] K. Shiozaki, H. Shapourian, and S. Ryu, Many-body topological invariants in fermionic symmetry-protected topological phases: Cases of point group symmetries, Phys. Rev. B **95**, 205139 (2017).